Journal of Colloid and Interface Science 624 (2022) 370–376

Contents lists available at ScienceDirect

Journal of Colloid and Interface Science

journal homepage: www.elsevier.com/locate/jcis

Imbibition-induced ultrafast assembly and printing of colloidal photonic crystals

Weibin Li *, Chen Zhang, Ding Lan, Wenjie Ji, Zhongyu Zheng, Yuren Wang *

National Microgravity Laboratory, Institute of Mechanics, Chinese Academy of Sciences, 100190 Beijing, China
School of Engineering Science, University of Chinese Academy of Sciences, 100049 Beijing, China

GRAPHICAL ABSTRACT

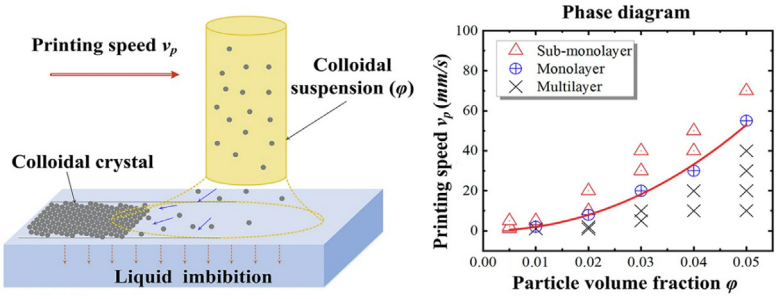

ARTICLE INFO

Article history:
Received 16 January 2022
Revised 17 May 2022
Accepted 18 May 2022
Available online 21 May 2022

Keywords:
Printing
Self-assembly
Colloidal crystal
Liquid imbibition
Photonic crystal

ABSTRACT

Hypothesis: Self-assembly of colloidal particles enables the versatile fabrication of highly ordered structures and materials for optical, sensing, and other applications. Nevertheless, many traditional assembly processes are inefficient, because there exists an inevitable contradiction between time efficiency and crystalline quality. In this work, we introduce an ultrafast, robust, and scalable approach of imbibition-induced assembly. We assume that the instantaneous solvent imbibition induced by the nanoporous media could direct ultrafast self-assembly of colloidal particles into ordered structures.
Experiments: Self-assembly of colloidal particles from a droplet on a nanoporous substrate was firstly observed and investigated. A phase diagram of the thickness of the colloidal crystal as a function of the printing speed and the particle volume fraction was presented through systematic experiments.
Findings: The nanoporous substrate can induce strong capillary flow that will direct the rapid self-assembly of particles into colloidal crystals. The imbibition-induced assembly was spatially and temporally combined with the meniscus-guided printing approach, and the printing speed can be improved by two orders of magnitude than the traditional evaporative assembly methods. We finally demonstrate an effective and ultrafast approach for assembling colloidal particles into photonic crystals with controllable sizes and shapes on the macroscale.

1. Introduction

Artificial materials exhibit unique optical [1,2], electrical [3], thermal [4], and mechanical [5] properties based on the diverse composition, configuration, and arrangement of the building blocks, which promote the development of a wide variety of appli-

* Corresponding authors.
E-mail addresses: liweibin@imech.ac.cn (W. Li), yurenwang@imech.ac.cn (Y. Wang).

https://doi.org/10.1016/j.jcis.2022.05.114
0021-9797/

cations, including colloidal photonic crystals [6,7], flexible colloidal nanocrystal electronics [8,9], biochemical sensors [10], wearable products [11], etc. As a simple and low-cost approach, self-assembly is one of the few practical strategies for establishing this kind of ordered materials such as colloidal crystals. Over the decades, scientists have developed many approaches to assemble colloidal particles into crystalline arrays, such as the Langmuir–Blodgett (LB) technique [12], dip-coating [13], spin-coating [14], vertical deposition [15], sedimentation [16], microfluidic [17] and patterned substrate [18]. However, it is difficult to fabricate colloidal crystals with controllable sizes and shapes without the assistance of a template for these approaches.

Evaporative self-assembly based on inkjet printing offers a non-lithographic means to produce multifarious and patterned colloidal crystals [19,20]. During printing, the self-assembly process is tightly coupled with the complex flow and transport of an evaporating droplet, which includes the outward capillary flow [21,22], thermal or solutal Marangoni flow [23,24], diffusion, and Brownian motion. Evaporative self-assembly is a result of the interplay of these various forces from different origins and with diverse magnitudes [25]. However, the colloidal particles under the forces of fluid flows are far from equilibrium, so they move so fast and tend to form non-uniform and disordered structures, such as ring-like patterns or clumps in the interior [26–28]. Despite recent works revealing that colloidal particles have enough time to arrange and self-assemble into ordered structures under Brownian motion or diffusion relying on interfaces [29,30], the preparation efficiency is inevitably restricted. A problem of the contradiction between quality (ordered phases) and efficiency (high assembly rate) in evaporative assembly arises. It will further influence the spatio-temporal mismatch between assembly and printing.

Here, we introduce an ultrafast imbibition process to enhance the assembly rate and suppress the complex processes of convection and transport induced by evaporation. It makes colloidal particles self-assemble into ordered structures on the nanoporous surface in a few seconds, which is far faster than the approach of evaporative self-assembly [29,30]. This solvent imbibition-induced self-assembly (IISA) was further combined with the meniscus-guided printing (MGP) technique to establish an effective and ultrafast approach for assembling and printing patterned colloidal crystals.

2. Materials and methods

2.1. Fabrication of nanoporous substrate

The nanoporous substrates were prepared by evaporation of colloidal silica suspensions (Ludox SM-30, Sigma-Aldrich). The mass fraction of the suspension is 30 wt%, the diameter of the silica particle is 12 nm. A culture dish was chosen as a mold for containing the suspensions of colloidal silica. After about 2 days of slow evaporation in a closed environment, it can be formed the nanoporous substrate inside the culture dish. The porosity of the substrate can be estimated to be 30%.

2.2. Preparation of colloidal suspensions

The colloidal suspensions of polystyrene (*PS*) in this work, purchased from Duke Scientific Corporation (5200A), have an initial mass concentration of 10 wt. % and density of 1.05 g/cm^3. The particle sizes (diameters) ranges from 170, 180, 230, 255, 320, 1000 and 3000 nm. Before we start experiments, the colloidal suspensions were first diluted 2 to10 times by ultra-pure water, and then the suspensions were stirred by ultrasonic for 1 min to ensure the uniform dispersion of particles.

2.3. Apparatus for liquid dispensing and printing

An electronic syringe for direct dosing system (Dataphysics, IDS) equipped with a disposable dosing needle was adopted for injecting colloidal suspensions. The injection process was motor-driven and software-controlled. The needle (SNS-D 051/025, with an inner diameter of 0.25 mm and outer diameter of 0.51 mm), was treated as hydrophobic to prevent the aqueous solution from climbing. The injection rate of the syringe was set in the range of 0.1 to 1 μL/s. The electronic syringe system is integrated with a three-dimensional (3D) displacement platform. When the needle and the nanoporous substrate move relatively, the suspensions can be printed and colloidal crystal films can be formed.

2.4. In situ observation of the assembly process

Droplet imbibition and colloidal assembly occur instantaneously, therefore, high-speed photography was adopted to observe the ultrafast dynamic process. The self-assembly of colloidal particles on the nanoporous substrate was captured by a high-speed camera (AOS, TRI-VIT) connected to a microscope (OLYMPUS, BX3M) from the top-view at 1000 fps. The injection, spreading, and imbibition processes of a colloidal droplet on the substrate were simultaneously captured by a side-view CCD camera (Dataphysics, IDS); 120 frames per second were used.

2.5. Characterizations of morphology

A transmitting and reflecting optical microscopy was used for observing the morphology of colloidal crystals with micrometer-size particles. The morphology of the printed patterns with submicron particles was characterized by an ultrahigh-resolution scanning electron microscope (HITACHI SU-70 FE-SEM) with 5 kV and 4∼5 mm scanning distance. A fiber optic spectrometer (Avaspec-2048, Avantes, Netherlands) coupled to a reflection probe was used for spectrum analysis, where the incident and reflective angles were both fixed at 0°.

3. Results and discussion

3.1. IISA of colloidal particles

The IISA is examined by injecting a sessile colloidal droplet on the nanoporous substrate (The nanoporous surface can be seen in Fig.S1, Supporting Information). The temporal and spatial evolution of the colloidal droplet is essential for revealing the mechanisms of IISA. After injection, the droplet evolves into three distinct stages according to the dynamic behavior of the contact line: spreading, pinning, and dewetting (Fig. 1a), which can be further quantitatively described through the time evolution of contact radius from a high-speed photographic experiment, as shown in (Fig. 1c). The time scales for the three stages range from milliseconds ($\sim 10^{-3}s$) to seconds ($\sim 10^{0}s$). The liquid spreading (stage I) is so fast that there is no enough time for the solvent to be absorbed by the nanoporous substrate. The sizes and areas of the final patterns can be determined by this spreading stage.

In the pinning stage, the contact angle continues to decrease but the contact line remains pinned (Fig. 1c). The solvent continues to be imbibed by the porous substrate for several seconds. As shown in (Fig. 2f), the vertical imbibition will induce the downward flow inside the droplet, which will carry the particles toward the solid surface. The lateral imbibition near the contact line will induce the outward flow towards the edge of the droplet [31], and colloidal particles will be transported and form ring-like structure (Fig. 1b & Fig. 2b,c). It is similar to the "coffee ring" effect caused

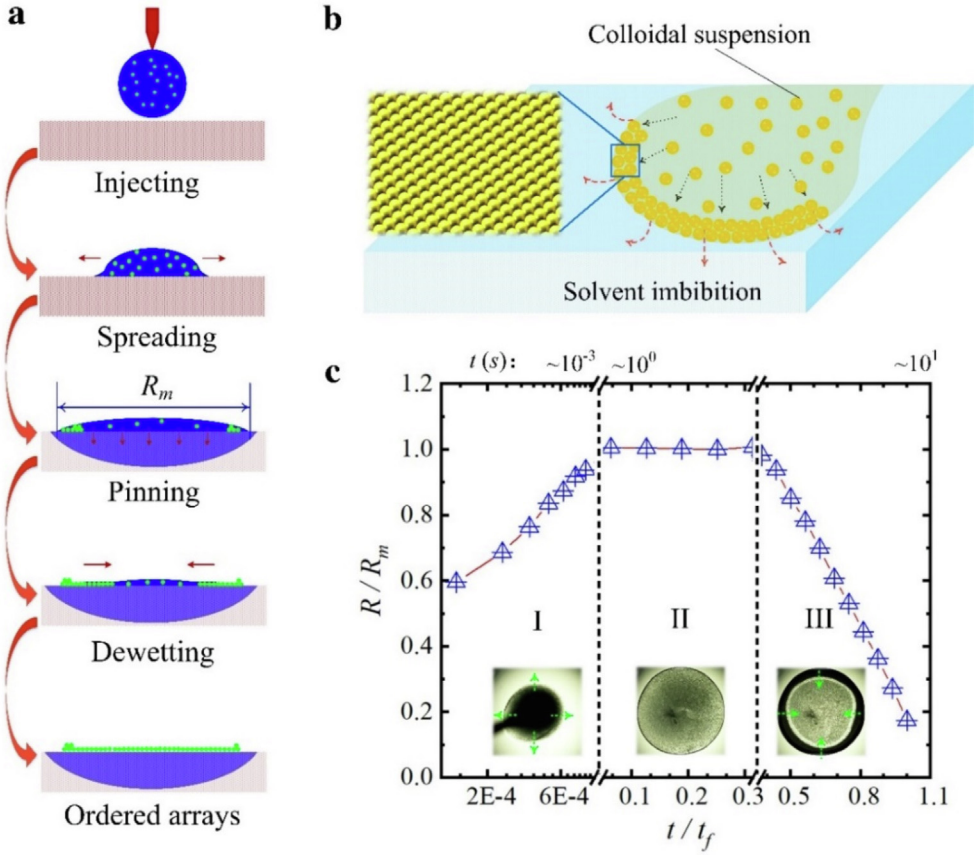

Fig. 1. (a) Schematics of spreading, pinning, and dewetting from an injected droplet on a nanoporous substrate. (b) Schematics of the IISA of colloidal particles and formation of ordered arrays. (c) The dimensionless contact radius (R/R_m) as a function of the dimensionless time (t/t_f) from a high-speed photographic experiment, where R_m and t_f represent the maximum contact radius and the final time for imbibition, respectively. It can be divided into three typical stages for the interactions of the liquid and solid: spreading, pinning, and dewetting. The time scales for these three stages range from milliseconds to seconds. The microscopic images at different stages are inserted.

by non-uniform evaporation flux revealed by Deegan et al. [21], however, the time scale for evaporation is far larger than imbibition [31], so the evaporation effect can be negligible. It's noteworthy that this ring has multilayer ordered structures (Fig. S2, Supporting Information) Fig.S3, which is different from the ring-shaped stain ranging from order to disorder caused by evaporation [32]. The formation of the ordered structures can be attributed to the guidance of the nanoporous substrate and constraint of the liquid–air interface.

As with solvent imbibition, the droplet eventually evolves into a thin liquid film whose thickness is roughly equal to the particle size, i.e., particles are constrained between the liquid–air and liquid–solid interface. Liquid film dewetting occurs from the edge toward the center and the contact line shrinks inward. During the evolution of dewetting, the outward flow increases rapidly because there is very little solvent left while the lateral imbibition flux remains unchanged. Therefore, as shown in (Fig. 2a), the particles will be transported towards the contact line (the dotted white line) instantaneously under the force of the capillary flow (the red arrow lines). These particles will assemble into an ordered monolayer structure under the capillary immersion forces, as shown in the enlarged image of (Fig. 2g). Here, the formation speed of monolayer ordered structures in (Fig. 2a) is about 0.6 mm·s^{-1}, which is significantly faster than traditional convective assembly [33]. The large area of ordered monolayer structures inside the ring can be seen in (Fig. 2b, d). The monolayer has a two-dimensional (2-D) polycrystalline structure where every single grain has a hexagonal closed-packed (HCP) array (Fig. 2e). The white radial wavy lines in (Fig. 2b), representing the colloidal grain boundaries, is another experimental evidence of the outward capillary flow. By adjusting the particle volume fraction and droplet size, a large area of monolayer colloidal crystal can be rapidly fabricated (Fig.S3, Supporting Information). Because of the strong flow behavior induced by imbibition and the uneven nanoporous surface, it emerges inevitable defects such as vacancies and grain boundaries in colloidal crystals, as shown in (Fig. 2e).

3.2. Ultrafast printing of colloidal crystals by using IISA

The above results indicate that solvent imbibition through nanoporous media offers a rapid way to self-assemble colloidal particles into ordered structures. To further fabricate any shaped and large-scale ordered arrays that are not limited to circular patterns, this IISA approach was combined with the MGP technique, as shown in (Fig. 3a). When the colloidal suspension is dispensed through the needle and contacts the porous substrate, it forms a meniscus between the needle and the porous substrate. As the substrate moves, the receding liquid meniscus evolves into a thin liquid film instantaneously, which accelerates the outward capillary flow induced by lateral solvent imbibition. The colloidal particles will be fastly carried towards the bilateral contact lines of the printed liquid film under the capillary flow, and finally self-assembled into ordered arrays under the capillary immersion forces. Theoretically, complex freeform shapes can be printed through the mobile stages in principle. Here, a multilayer arc-shaped pattern was printed, as shown in (Fig. 3b). We also created a large-scale strip-line pattern with a length of 13 cm (Fig. 3c),

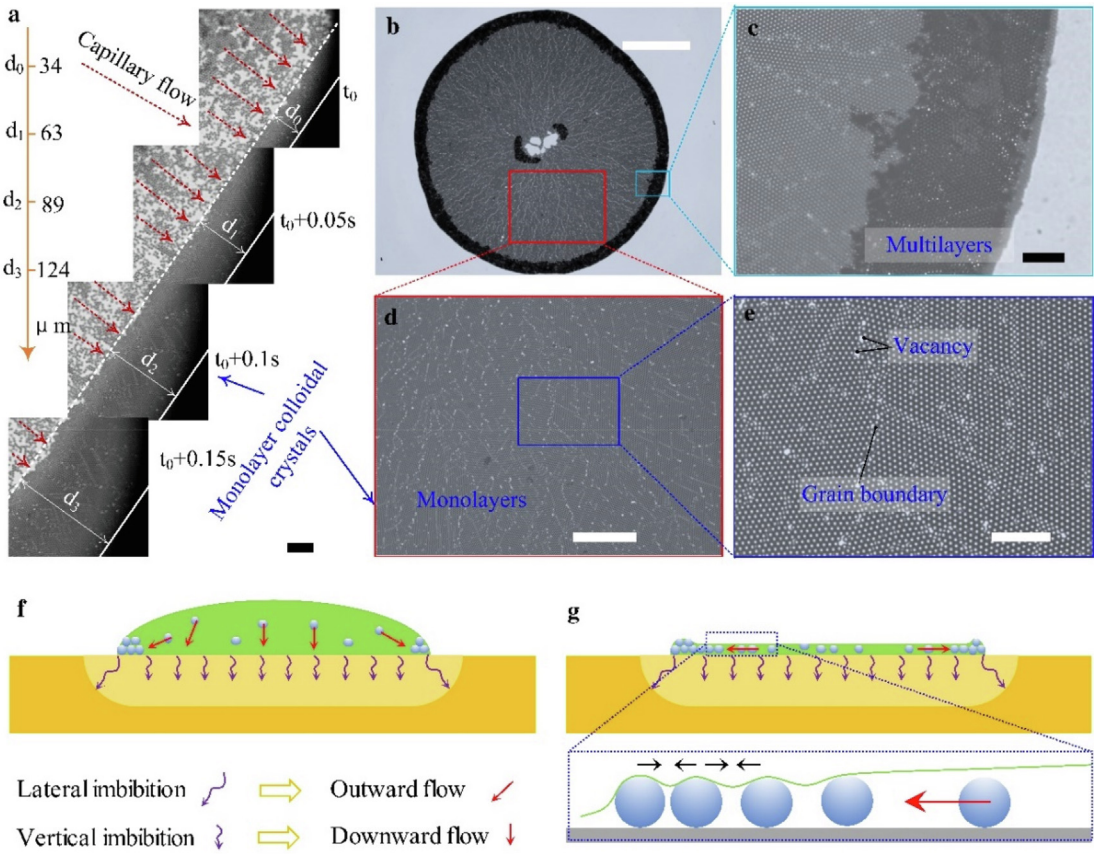

Fig. 2. Optical micrographs of the IISA of colloidal particles and the resulting structures under different magnification, the initial volume and concentrations of the droplet are 0.5 μL and 2 wt%, respectively. (a) Imbibition directed self-assembly of particles and formation process of the ordered monolayer structures as with time, the dotted white line represents the interface between particle arrays and fluids (contact lines), the red arrows represent the micro-flow toward the contact line, d_0-d_3 reflect the formation speed of monolayer colloidal crystals. (b) Patterns formed on a porous substrate from an imbibed droplet. (c) The enlarged ring stain has ordered structures. (d-e) Ordered array monolayer structure inside the ring stain, the white dots and lines represent vacancies and grain boundaries, respectively. Scale bars of (a-e) are 30, 500, 30, 120, 30 μm, respectively. (f-g) Schematic of the outward and downward flow caused by lateral and vertical imbibition, respectively. The enlarged image of (g) represents the capillary immersion forces between the adjacent particles.

which contains multilayer edges (Fig. 3d-e) and monolayer intermediate regions (Fig. 3f-g).

The IISA assisted printing process can be further described quantitatively. As the stage moves at a constant speed (v_p) along the *x*-axis, 2D colloidal crystals will be stably and continuously formed on the nanoporous substrate, as shown in (Fig. 4a). Based on the comparative analysis of convective assembling of particles into 2D colloidal arrays induced by evaporation [34], the material flux balance was used to describe the dynamic process of the IISA. Considering the solvent imbibition flux, J_i, is exactly compensated by the water flow from the bulk suspension into the arrays, J_w, thus the rate of the crystal growth v_c can be derived as

$$v_c = \frac{\beta l j_i \varphi}{h(1-\varepsilon)(1-\varphi)} \tag{1}$$

Where h is the thickness of the colloidal films, φ is the particle volume fraction of the colloidal suspensions, ε is the porosity of the colloidal crystals, l is an imbibition length defined as $l = J_i/j_i$, J_i is the total solvent imbibition flux, j_i is the average imbibition flux of solvent from the nanoporous substrate, β is the hydrodynamic parameter defined as the velocity ratio of the water molecule to the particle. Detailed derivation can be referred to the literature [34]. The average imbibition flux j_i can be calculated from Darcy's Law [35]:

$$j_i = kP_c/\mu h_c \tag{2}$$

where k is the permeability of the porous substrate, which can be deduced from the Kozeny-Carman law, μ is the fluid viscosity, P_c is the capillary pressure simplified as $P_c \sim \gamma/a$, where γ is the solvent interfacial tension, a is the radius of the colloidal silica particles. h_c is the characteristic length of imbibition and can be expressed as

$$h_c = \frac{h(1-\varepsilon)(1-\varphi)}{\varphi} \tag{3}$$

By substituting j_i from eq (2) and h_c from eq (3) into eq (1), the rate of the crystal growth can be expressed as

$$v_c = \frac{\beta l k P_c \varphi^2}{h^2 \mu (1-\varepsilon)^2 (1-\varphi)^2} \tag{4}$$

Then, for the formation of monolayers close-packed structures ($h = d$, where d is the diameter of the particles), the printing speed (the withdrawal rate of the substrate) v_p is equal to the rate of the crystal growth v_c.

$$v_p = \frac{\beta l k P_c \varphi^2}{d^2 \mu (1-\varepsilon)^2 (1-\varphi)^2} \tag{5}$$

A phase diagram where the sub-monolayer, monolayer, and multilayer structures are plotted as a function of φ and v_p (Fig. 4b). The red line represents the theoretical curves of eq (5), as the parameters of $\beta = 1$, $l = 5.6$ mm, $k = 4.4 \times 10^{-20}$ m^2, $P_c \sim \gamma/a = 1.2 \times 10^7$ N/m^2 ($\gamma = 72$ mN/m, a = 6 nm), $d = 1$ μm, $\mu = 10^{-3}$

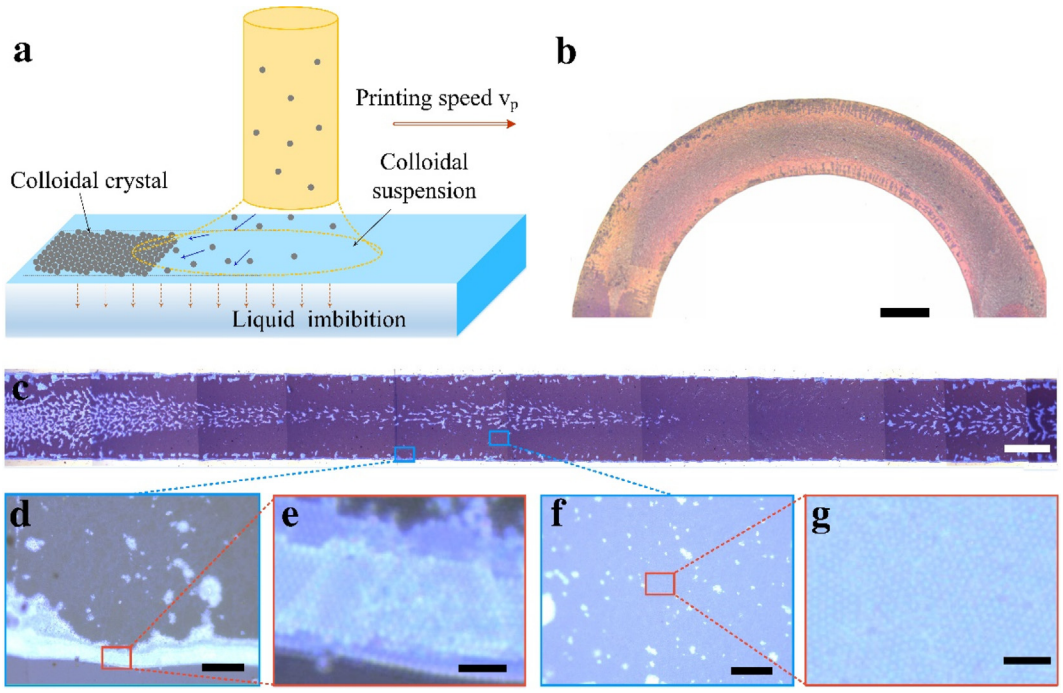

Fig. 3. (a) Schematic of the IISA-assisted MGP method for the fabrication of colloidal crystals. (b) An arc-shaped pattern was printed, the particle size is 500 nm and the scale bar is 0.6 mm. (c) A strip-line pattern was printed, the particle size is 1 μm and the scale bar is 0.6 mm. (d, f) are enlarged figures of the sky-blue rectangles in (c), the scale bars are 40 μm. (e, g) are enlarged images of the red rectangles in (d) and (f), respectively, Tthe scale bars are 5 μm.

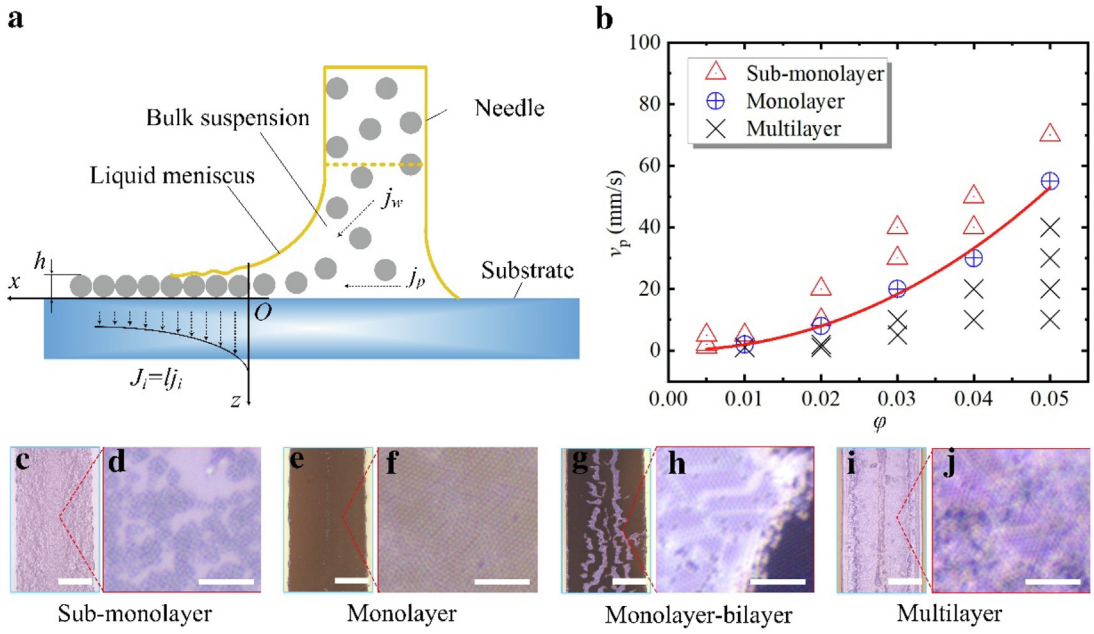

Fig. 4. (a) Schematic diagram of convective flux induced by solvent imbibition during MGP. (b) A phase diagram where sub-monolayer, monolayer, and multilayer phases are plotted as a function of the particle volume fraction φ and the printing speed v_p. (c-j) The reflection optical micrographs of the printed sub-monolayer (c,d), monolayer (e,f), monolayer-bilayer (g,h) and multilayer (i, j) structures as the increase of the particle volume fractions (From left to right: 2%, 3%, 4%, 5%) when the printing speed v_p is 20 mm/s. (d, f, h, j) are enlarged optical micrographs from specific regions of (c, e, g, i), respectively. The particle diameter is 1 μm. The scale bars of (c, e, g, i) are 400 μm, the scale bars of (d, f, h, j) are 10 μm.

Pa·s, $\varepsilon = 0.605$. The printing speed increases nonlinearly as with the increase of the particle volume fraction (φ). The experimental circle points (○) representing the monolayer structures collapse onto the theoretical value. When φ is constant, the lower the printing speed, the more easily the multilayer structures can be formed, as shown in the cross sign (×) below the red line; the higher the printing speed, the more easily the sub-monolayer structures can be formed, as shown in the triangle sign (△) above the red line. The detailed morphology of the printed lines are shown in Fig. 4, including the sub-monolayer (Fig. 4c,d), monolayer (Fig. 4e,f), monolayer and bilayer (Fig. 4g,h) and multilayer structures (Fig. 4i,j) (v_p is 20 mm/s; φ is 2%, 3%, 4% and 5%, respectively). From

the diagram in (Fig. 4b), the printing speed, i.e., the growth speed of monolayer colloidal crystals induced by imbibition, is improved by two orders of magnitude than evaporative assembly methods [36,37]. The ultrafast printing of colloidal crystals can be attributed to the accelerating imbibition caused by a thin film at the trailing end of the receding liquid meniscus (Fig. 4a). The ordered structures with different morphology and thickness can be quickly printed and easily controlled by coordinating the printing speed, the particle sizes, and the volume fractions of particles. (Fig. 4e, f) shows the typical monolayer colloidal crystals under the conditions of φ = 0.03, v_p = 20 mm/s and d = 1 μm. Therefore, the integration of the IISA and MGP offers an ultrafast and effective way to fabricate specific shaped and large-scale ordered structures.

3.3. The optical performance of colloidal crystals fabricated by IISA

The printed colloidal crystals appear a periodically ordered microstructure (Fig.S4, Supporting Information) which can reflect structural coloration due to Bragg reflection [17]. As shown in (Fig. 5a), we fabricated colloidal crystals that exhibit different colors depending on the size of the particles. Upon white light illumination, colloidal crystals formed from particle sizes of 170, 180, 230, 255, and 320 nm present diverse structural colors. Reflectance spectroscopy reveals Bragg reflection peaks at wavelengths of 386, 410, 546, 602, and 744 nm, respectively. It's basically the same wavelength as Bragg's law (Table S1, Supporting Information). This implies the possibility of building macroscale colloidal crystals with tailored optical properties by choosing specific particle sizes and compositions. The lower reflectance peaks can be attributed to a high density of defects, as shown in (Fig. 5b-f), which can be observed from the SEM images of the printed colloidal crystals formed from particle sizes of 170, 180, 230, 255, and 320 nm, respectively. It suggests that IISA offers an effective approach to construct ordered structures for particles with sizes ranging from the nanoscale to the microscale, and this ordered colloidal crystal can be transferred from the nanoporous surface layer by layer to form monolayer structures onto the soft Polydimethylsiloxane (PDMS) substrate, as shown in (Fig. 5g, h). It still exhibits typical colors under specific incident angles (Fig. 5i). Therefore, this approach has potential applications in flexible photonic crystals and wearable devices.

4. Conclusion

A new concept of IISA is proposed in this work, and an ultrafast, robust, and scalable approach is further developed for printing colloidal crystals. The imbibition caused by the nanoporous substrate, which breaks the quasi-steady state evaporation and suppresses the complex processes of convection and transport, can induce ultrafast capillary flows that will direct the colloidal particles self-assemble into ordered structures. Furthermore, the IISA is spatial and temporal combined with the MGP approach to fabricate patterned colloidal crystals. An operational phase diagram was constructed that could quantitatively describe structures of the printed film as a function of printing speed and particle volume fractions. Finally, colloidal photonic crystals with diverse structural colors were rapidly assembled and printed by using this approach. To a certain extent, the contradiction between time efficiency and crystalline quality in colloidal crystal preparation can be solved by this approach.

Convective assembly of colloidal particles has been widely studied in recent years, and many approaches relying on liquid meniscus evaporation were developed such as vertical deposition [15,34,38,39], horizontal deposition [36,40], and direct writing [37,41,42]. However, evaporative assembly for these techniques is so slow that seriously affects the growth rate. The spin-coating was used for rapidly fabricating high-quality and large-area colloidal crystals [14], but it is difficult to print patterned colloidal crystal directly without a template. By introducing the imbibition effect into the conventional MGP, the printing speed can be remarkably improved by at least two orders of magnitude than the traditional methods of evaporative assembly [36,37] (Table 1). This strategy offers a simple and highly efficient way of printing multiscale ordered structures and creating functional surface patterns. In the future, this approach needs further optimization for printing high-quality, large-area, and even 3D colloidal crystals. The application of the imbibition-assisted roll-to-roll manufacturing of flexible colloidal crystals films and printing of wearable optical sensors can be necessary to be explored.

CRediT authorship contribution statement

Weibin Li: Conceptualization, Methodology, Investigation, Visualization, Data curation, Formal analysis, Funding acquisition,

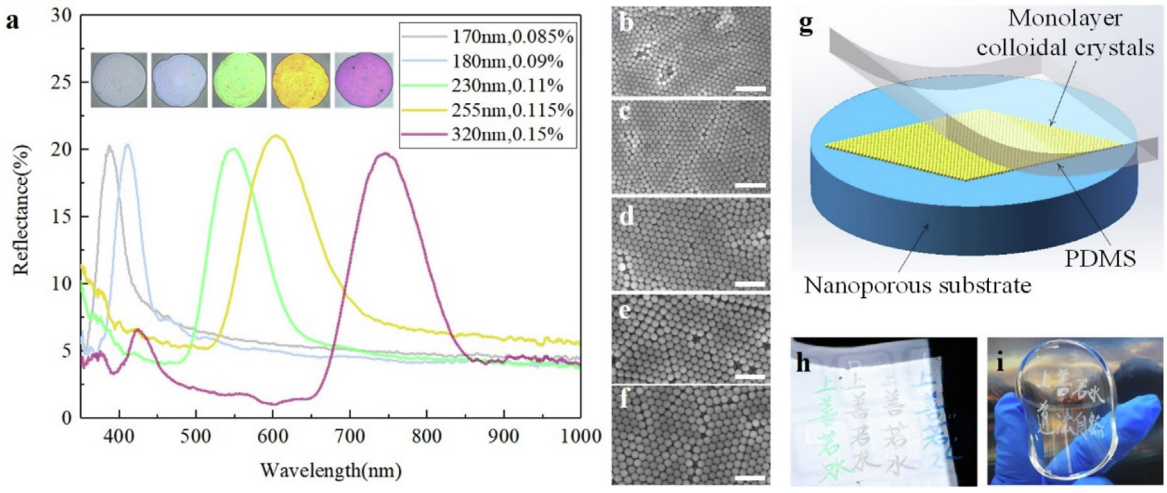

Fig. 5. (a) Colloidal crystals with structural colors tunable by the sizes of PS particles (170, 180, 230, 255, and 320 nm) and mass fraction of colloidal suspensions (0.085%, 0.09%, 0.11%, 0.115%, and 0.15%) under white-light illumination, and corresponding reflectance spectra measured from the surface of each of the above structures. (b-f) SEM images of the ordered structures with particle sizes of 170 nm, 180 nm, 230 nm, 255 nm, and 320 nm. The scale bars of (b–f) are 1 μm. (g) Schematic of the colloidal crystals (the yellow part) being transferred from the nanoporous substrate onto the soft PDMS. (h,i) The structural colors of the patterns of colloidal photonic crystals on the PDMS.

Table 1
Comparison of the printing (coating) speed (μm/s) of diverse meniscus-guided printing approaches for preparation of monolayer colloidal crystals.

Methods\volume fractions	**0.025**	**0.03**	**0.05**	**0.1**	**0.2**
Meniscus guided coating [36]	—	~5	~10	~20	~40
Direct-write printing [37]	~50	~100	~150	~300	~600
This work	~10000	~200000	~50000	—	—

Writing – original draft, Writing – review & editing. **Chen Zhang:** Visualization, Investigation. **Ding Lan:** Visualization. **Wenjie Ji:** Visualization. **Zhongyu Zheng:** Writing – review & editing. **Yuren Wang:** Resources, Project administration, Funding acquisition, Writing – review & editing, Conceptualization.

Declaration of Competing Interest

The authors declare that they have no known competing financial interests or personal relationships that could have appeared to influence the work reported in this paper.

Acknowledgements

The authors gratefully acknowledge financial support from the National Natural Science Foundation of China (Grant No. 11902321) and Basic Research Program of Manned space Station of Chinese Academy of Sciences (Grant No. ZDBS-ZRKJZ-TLC014).

Appendix A. Supplementary material

Supplementary data to this article can be found online at https://doi.org/10.1016/j.jcis.2022.05.114.

References

[1] Y. Wang, I.C. Jenkins, J.T. McGinley, T. Sinno, J.C. Crocker, Colloidal crystals with diamond symmetry at optical lengthscales, Nat. Commun. 8 (1) (2017) 1–8.
[2] Z. Xie, K. Cao, Y. Zhao, L. Bai, H. Gu, H. Xu, Z.Z. Gu, An optical nose chip based on mesoporous colloidal photonic crystal beads, Adv. Mater. 26 (15) (2014) 2413–2418.
[3] C. Mao, J. Huang, Y. Zhu, W. Jiang, Q. Tang, X. Ma, Tailored parallel graphene stripes in plastic film with conductive anisotropy by shear-induced self-assembly, The journal of physical chemistry letters 4 (1) (2013) 43–47.
[4] H. Zeng, J. Wu, Y. Ma, Y. Ye, J. Liu, X. Li, Y. Wang, Y. Liao, X. Luo, X. Xie, Y.-W. Mai, interfaces, Scalable approach to construct self-assembled graphene-based films with an ordered structure for thermal management, ACS Appl. Mater. Interfaces 10 (48) (2018) 41690–41698.
[5] X.W. Gu, X. Ye, D.M. Koshy, S. Vachhani, P. Hosemann, A.P. Alivisatos, Tolerance to structural disorder and tunable mechanical behavior in self-assembled superlattices of polymer-grafted nanocrystals, Proceedings of the National Academy of Sciences 114(11) (2017) 2836-2841.
[6] J. Hou, M. Li, Y. Song, Recent advances in colloidal photonic crystal sensors: materials, structures and analysis methods, Nano Today 22 (2018) 132–144.
[7] P. Di Palma, C. Taddei, A. Borriello, G. De Luca, M. Giordano, A. Iadicicco, S. Campopiano, L. Sansone, Self-assembled colloidal photonic crystal on the fiber optic tip as a sensing probe, IEEE Photonics J. 9 (2) (2017) 1–11.
[8] C.R. Kagan, Flexible colloidal nanocrystal electronics, Chem. Soc. Rev. 48 (6) (2019) 1626–1641.
[9] J.-H. Choi, H. Wang, S.J. Oh, T. Paik, P. Sung, J. Sung, X. Ye, T. Zhao, B.T. Diroll, C. B. Murray, C.R. Kagan, Exploiting the colloidal nanocrystal library to construct electronic devices, Science 352 (6282) (2016) 205–208.
[10] C. Fenzl, T. Hirsch, O.S. Wolfbeis, Photonic crystals for chemical sensing and biosensing, Angew. Chem. Int. Ed. 53 (13) (2014) 3318–3335.
[11] W.S. Lee, S. Jeon, S.J. Oh, Wearable sensors based on colloidal nanocrystals, Nano Convergence 6 (1) (2019) 10.
[12] M. Szekeres, O. Kamalin, R.A. Schoonheydt, K. Wostyn, K. Clays, A. Persoons, I. Dékány, Ordering and optical properties of monolayers and multilayers of silica spheres deposited by the Langmuir-Blodgett method, J. Mater. Chem. C 12 (11) (2002) 3268–3274.
[13] M. Ghosh, F. Fan, K.J. Stebe, Spontaneous pattern formation by dip coating of colloidal suspensions on homogeneous surfaces, Langmuir 23 (4) (2007) 2180–2183.
[14] P. Jiang, M.J. McFarland, Large-scale fabrication of wafer-size colloidal crystals, macroporous polymers and nanocomposites by spin-coating, J. Am. Chem. Soc. 126 (42) (2004) 13778–13786.
[15] J.-M. Meijer, F. Hagemans, L. Rossi, D.V. Byelov, S.I. Castillo, A. Snigirev, I. Snigireva, A.P. Philipse, A.V. Petukhov, Self-assembly of colloidal cubes via vertical deposition, Langmuir 28 (20) (2012) 7631–7638.
[16] Y. Li, L. Zhou, G. Liu, L. Chai, Q. Fan, J. Shao, Study on the fabrication of composite photonic crystals with high structural stability by co-sedimentation self-assembly on fabric substrates, Appl. Surf. Sci. 444 (2018) 145–153.
[17] F. Bian, L. Sun, L. Cai, Y. Wang, Y. Wang, Y. Zhao, Colloidal Crystals from Microfluidics, Small 16 (9) (2020) 1903931.
[18] J. Hou, M. Li, Y. Song, Patterned colloidal photonic crystals, Angew. Chem. Int. Ed. 57 (10) (2018) 2544–2553.
[19] H. Nam, K. Song, D. Ha, T. Kim, Inkjet printing based mono-layered photonic crystal patterning for anti-counterfeiting structural colors, Scientific reports 6 (2016) 30885.
[20] K.N. Al-Milaji, R.R. Secondo, T.N. Ng, N. Kinsey, H. Zhao, Interfacial Self-Assembly of Colloidal Nanoparticles in Dual-Droplet Inkjet Printing, Adv. Mater. Interfaces 5 (10) (2018) 1701561.
[21] R.D. Deegan, O. Bakajin, T.F. Dupont, G. Huber, S.R. Nagel, T.A. Witten, Capillary flow as the cause of ring stains from dried liquid drops, Nature 389 (6653) (1997) 827–829.
[22] R.D. Deegan, O. Bakajin, T.F. Dupont, G. Huber, S.R. Nagel, T.A. Witten, Contact line deposits in an evaporating drop, Phys. Rev. E 62 (1) (2000) 756–765.
[23] H. Hu, R.G. Larson, Marangoni effect reverses coffee-ring depositions, J. Phys. Chem. B 110 (14) (2006) 7090–7094.
[24] H. Kim, F. Boulogne, E. Um, I. Jacobi, E. Button, H.A. Stone, Controlled uniform coating from the interplay of Marangoni flows and surface-adsorbed macromolecules, Phys. Rev. Lett. 116 (12) (2016) 124501.
[25] Q. Li, U. Jonas, X.S. Zhao, M. Kappl, The forces at work in colloidal self-assembly: a review on fundamental interactions between colloidal particles, Asia-Pac. J. Chem. Eng. 3 (3) (2008).
[26] R.G. Larson, Transport and deposition patterns in drying sessile droplets, AIChE J. 60 (5) (2014) 1538–1571.
[27] X. Man, M. Doi, Ring to Mountain Transition in Deposition Pattern of Drying Droplets, Phys. Rev. Lett. 116 (6) (2016) 066101.
[28] R.G.J.N. Larson, In Retrospect: Twenty years of drying droplets 550 (7677) (2017) 466–467.
[29] Y. Li, Q. Yang, M. Li, Y. Song, Rate-dependent interface capture beyond the coffee-ring effect, Sci. Rep. 6 (1) (2016) 1–8.
[30] W. Li, W. Ji, D. Lan, Y. Wang, Self-assembly of ordered microparticle monolayers from drying a droplet on a liquid substrate, The Journal of Physical Chemistry Letters 10 (20) (2019) 6184–6188.
[31] R. Dou, B. Derby, Formation of Coffee Stains on Porous Surfaces, Langmuir 28 (12) (2012) 5331–5338.
[32] Á.G. Marín, H. Gelderblom, D. Lohse, J.H. Snoeijer, Order-to-disorder transition in ring-shaped colloidal stains, Phys. Rev. Lett. 107 (8) (2011) 085502.
[33] L. Malaquin, T. Kraus, H. Schmid, E. Delamarche, H. Wolf, Controlled particle placement through convective and capillary assembly, Langmuir 23 (23) (2007) 11513–11521.
[34] A.S. Dimitrov, K. Nagayama, Continuous convective assembling of fine particles into two-dimensional arrays on solid surfaces, Langmuir 12 (5) (1996) 1303–1311.
[35] Y. Wang, Z. Liu, F. Muzzio, G. Drazer, G. Callegari, A drop penetration method to measure powder blend wettability, Int. J. Pharm. 538 (1–2) (2018) 112–118.
[36] B.G. Prevo, O.D. Velev, Controlled, Rapid Deposition of Structured Coatings from Micro- and Nanoparticle Suspensions, Langmuir 20 (6) (2004) 2099–2107.
[37] A.T. Tan, S. Nagelberg, E. Chang-Davidson, J. Tan, J.K. Yang, M. Kolle, A.J. Hart, In-Plane Direct-Write Assembly of Iridescent Colloidal Crystals, Small 16 (4) (2020) 1905519.
[38] Y. Suh, Q. Pham, B. Shao, Y. Won, The Control of Colloidal Grain Boundaries through Evaporative Vertical Self-Assembly, Small 15 (12) (2019) 1804523.
[39] P. Jiang, J. Bertone, K.S. Hwang, V. Colvin, Single-crystal colloidal multilayers of controlled thickness, Chem. Mater. 11 (8) (1999) 2132–2140.
[40] Z. Cai, J. Teng, Q. Yan, X. Zhao, Solvent effect on the self-assembly of colloidal microspheres via a horizontal deposition method, Colloids Surf., A 402 (2012) 37–44.
[41] B.F. Winhard, S. Haugg, R. Blick, G.A. Schneider, K.P. Furlan, Direct writing of colloidal suspensions onto inclined surfaces: Optimizing dispense volume for homogeneous structures, J. Colloid Interface Sci. 597 (2021) 137–148.
[42] Q. Li, J.A. Lewis, Nanoparticle inks for directed assembly of three-dimensional periodic structures, Adv. Mater. 15 (19) (2003) 1639–1643.